Above-room-temperature ferromagnetism in thin van der Waals flakes of cobalt-substituted Fe₅GeTe₂

Hang Chen^{1†}, Shahidul Asif^{2†}, Kapildeb Dolui³, Yang Wang¹, Jeyson Tamara Isaza^{1,4}, V. M. L. Durga Prasad Goli¹, Matthew Whalen¹, Xinhao Wang¹, Zhijie Chen⁵, Huiqin Zhang⁶, Kai Liu⁵, Deep Jariwala⁶, M. Benjamin Jungfleisch¹, Chitraleema Chakraborty^{1,2}, Andrew F. May⁷, Michael A. McGuire⁷, Branislav K. Nikolic¹, John Q. Xiao¹, Mark J.H. Ku^{1,2,*}

Key words: 2D magnetism, nitrogen vacancy centers, Co-substituted Fe5GeTe2, van der Waals magnets, quantum magnetic imaging

ABSTRACT

Two-dimensional (2D) magnetic van der Waals materials provide a powerful platform for studying fundamental physics of low-dimensional magnetism, engineering novel magnetic phases, and enabling thin and highly tunable spintronic devices. To realize high quality and practical devices for such applications, there is a critical need for robust 2D magnets with ordering temperatures above room temperature that can be created via exfoliation. Here the study of exfoliated flakes of cobalt substituted Fe₅GeTe₂ (CFGT) exhibiting magnetism above

¹Department of Physics and Astronomy, University of Delaware, Newark, Delaware 19716, United States

²Department of Materials Science and Engineering, University of Delaware, Newark, Delaware 19716, United States

³Lomare Technologies Ltd., 6 London Street, London EC3R 7LP, United Kingdom

⁴Departamento de Física, Universidad Nacional de Colombia, Bogotá D.C., Colombia

⁵Department of Physics, Georgetown University, Washington, DC 20057, United States

⁶Department of Electrical and Systems Engineering, University of Pennsylvania, Philadelphia, Pennsylvania 19104, United States

⁷Materials Science and Technology Division, Oak Ridge National Laboratory, Oak Ridge, Tennessee 37831, United States

room temperature is reported. Via quantum magnetic imaging with nitrogen-vacancy centers in diamond, ferromagnetism at room temperature was observed in CFGT flakes as thin as 16 nm corresponding to 16 layers. This result expands the portfolio of thin room-temperature 2D magnet flakes exfoliated from robust single crystals that reach a thickness regime relevant to practical spintronic applications. The Curie temperature $T_{\rm c}$ of CFGT ranges from 310 K in the thinnest flake studied to 328 K in the bulk. To investigate the prospect of high-temperature monolayer ferromagnetism, Monte Carlo calculations were performed which predicted a high value of $T_{\rm c} \sim 270$ K in CFGT monolayers. Pathways towards further enhancing monolayer $T_{\rm c}$ are discussed. These results support CFGT as a promising platform to realize high-quality room-temperature 2D magnet devices.

INTRODUCTION

The discovery of thin van der Waals (vdW) materials with magnetic ordering ¹⁻⁶ has opened up enormous opportunities for studying novel condensed matter phenomena and for meeting the demands of new information processing capabilities. Also known as two-dimensional (2D) magnets, they embody a high degree of tunability (e.g., via gating or strain), the ability to form custom-designed, multifunctional heterostructures, and the availability of a rich array of interfacial phenomena. These unique properties position 2D magnets as excellent platforms for fundamental study of low-dimensional spin physics⁷, engineering novel quantum phase via proximity effects⁶ or Moire structures⁸⁻¹⁰, and studying complex magnon behaviors^{11, 12}. The potential to realize these novel effects, together with the ability for highly efficient interfacial control¹³, present 2D magnets as promising platforms to implement a wide range of important applications from spintronics to magnon-based hybrid quantum systems^{14, 15}.

To realize high quality and practical devices for aforementioned applications, achieving a Curie temperature T_c above room-temperature presents a critical goal⁴. T_c significantly below room-temperature is common among 2D magnets; for example, $T_c \sim 60 \text{ K}$ in monolayer CrI_3^1 and CrGeTe_3^2 , and $\sim 130 \text{ K}$ in monolayer $\text{Fe}_3\text{GeTe}_2^{16}$. Recently, several works have reported magnetism at room-temperature or above in 2D magnetic flakes grown epitaxially, via chemical vapor deposition, or via chemical exfoliation¹⁷⁻²¹. However, materials prepared in such a way are often prone to disorder and are generally unsuitable for creating high quality devices. While wafer-scale growth processes such as epitaxy are necessary for future integration of 2D magnets in spintronic, optoelectronic, and quantum devices, it is imperative to gain understanding of high-quality samples to explore the applications possible in a given

material. To date, it is recognized that mechanical exfoliation from bulk material remains the technique of choice to achieve the highest quality in 2D devices, which has enabled the demonstration of an array of important capabilities ranging from low current-density spintorque switching¹³ to quantum anomalous Hall effect²² in 2D magnetic materials. This approach also enables newly discovered bulk materials to be screened rapidly. Among exfoliated flakes, Ref. 23 reports T_c above room temperature in ionically intercalated few-layer Fe₃GeTe₂, but controversy on the result remains²⁴; furthermore, ionic intercalation does not present a viable path for high quality devices. In the past few years, the possibility of intrinsic room-temperature ferromagnetism in exfoliated thin flakes is demonstrated in the 1T phase of CrTe₂^{25, 26} and 2H phase of VSe₂²⁷. However, there are potential robustness issues with these two vdW systems. In the case of VSe₂, its bulk crystal is not magnetic, but a structural phase transition occurs upon thinning and this leads to magnetic thin flakes²⁷. It is unknown whether this structural transition is sensitive to the substrate or to strain, which may present problems for heterostructure assembly and for creating devices. Furthermore, it can be desirable to create thin vdW magnetic flakes from a source material where the bulk crystal is magnetically ordered. For instance, the magnetic properties of the bulk offer a baseline for the expectations of the thinned material, and indeed detailed studies of the bulk are often required to understand the behavior of the thin flakes. The magnetic 1T-phase of CrTe₂ is meta-stable and decomposes above 330 K²⁵, which also presents an obstacle for heterostructure/device fabrication which generally requires heating above this temperature. Therefore, thin 2D magnets with T_c above room temperature created via exfoliation of robust crystals – thermally stable and magnetic in the bulk – present a highly sought-after goal. The possibility to realize 2D magnets with aforementioned properties is recently demonstrated in Fe₃GaTe₂ ²⁸. Following this breakthrough, there is an urgent need to expand the portfolio of such materials. In this work, we report above-room-temperature ferromagnetism in exfoliated flakes of Cosubstituted Fe₅GeTe₂. The family of iron-based vdW metals Fe_nGeTe₂ provides a promising platform for engineering high T_c 2D magnet, where T_c can be raised by increasing Fe content from n=3 to 5^{16, 29-31}. While Fe₅GeTe₂ system has a stacking related transition near 570K, the material appears to be thermally and structurally stable³². Fe₅GeTe₂-based system has a versatile feature that a rich array of diverse properties can be generated via Cobalt substitution, leading to significant interest in this family of material in the recent years³³⁻³⁷. High Co-content (>40%) can turn the system into either an antiferromagnet^{33, 34, 37} (demonstrated for bulk crystal) or a polar ferromagnet^{35, 36} (demonstrated for flakes down to 58 nm thickness). Intermediate Co- substitution (\sim 30%) is found to increase T_c in bulk crystal of Fe₅GeTe₂^{33, 34}, indicating the potential for above-room-temperature ferromagnetism in thin Fe₅GeTe₂ with intermediate Co-substitution (which we shall refer to as CFGT) flakes. However, thin flakes generally have lower T_c compared to bulk crystals, hence the question of whether thin CFGT flakes could exhibit room-temperature magnetism remains to be explored. We address this question by detecting the minute magnetic stray field signal of CFGT flakes in air at room-temperature and above with a novel quantum magnetic imaging (QMI) technique based on nitrogen-vacancy (NV) centers in diamond. We have observed ferromagnetism at room-temperature in flakes as thin as 16 nm (16 layers). Along with Fe₃GaTe₂²⁸, this corresponds to one of the only room-temperature 2D magnet flakes with thickness in the device-relevant regime exfoliated from robust single crystals. This result also corresponds to the thinnest flake with room-temperature ferromagnetic ordering among the family of Co-substituted Fe₅GeTe₂ materials. The measured Curie temperature of CFGT ranges from 310 K in the thinnest flake studied to 328 K in the bulk. To investigate the prospect of high-temperature monolayer ferromagnetism, Monte Carlo simulations using ab *initio* effective spin Hamiltonian have been employed to determine a nearly-room-temperature $T_c \sim 270 \text{ K}$ in CFGT monolayer. We discuss the prospect for further enhancing T_c in monolayer CFGT. Our results point to CFGT as a promising platform to realize high-quality devices operational at room-temperature for applications and fundamental studies. In terms of applications, the potential air-stability of Fe-Ge-Te thin flakes does present a challenge and this aspect will require dedicated investigations, such as in Ref. ³⁸; this work points to the value in further pursuing systematic investigation of CFGT thin flakes for room-temperature devices.

RESULTS AND DISCUSSION

Characterization of Bulk CFGT Crystal

CFGT crystal growth and structural information (Inset in **Figure 1**a) are reported previously³³. Crystals described in Ref. ³³ remain ferromagnetic and have an enhanced T_c ≈ 330 K up to $\approx 30\%$ Co-substitution; above this level of substitution, e.g. at $\approx 50\%$, the material becomes antiferromagnetic. We note that another work reports the realization of a polar ferromagnetic metal with 50% Co-substituted Fe₅GeTe₂³⁶. Difference between these two works may be due to minor differences in composition and the resulting structure. Material reported in Ref. ³⁶ also exhibits a high $T_c \approx 350$ K, but magnetic properties were only examined in flakes with thickness >100 nm. In the present work, the bulk CFGT corresponds

to the 28% Co-substituted crystals utilized in Ref. ³³. Specifically, the crystals are from the same crystal growth as the previously reported 28% Co-substituted crystals, where the cobalt content was determined from energy dispersive spectroscopy and was found to be consistent across the crystal growth products. In addition, single crystal x-ray diffraction was utilized to examine the crystal structure of products from this growth. Data shown in Fig. 17 of Ref ³⁹ also originated from crystals from this same growth, and the diffraction data demonstrated that the 28% Co-substituted samples have significant stacking disorder. Temperaturedependent magnetization measurements (Figure 1a) were performed with a vibrating sample magnetometer and reveals $T_c = 328 \text{ K}$ (for details on the extraction, refer to S4 in Supporting **Information**) for the bulk crystal, consistent with previous results³³. Isothermal magnetization data with demagnetization effect accounted for (see Section S5 in Supporting **Information** for details) is shown in **Figure 1**b which reveals easy-plane anisotropy, likewise consistent with the previous result³³. Furthermore, we extracted the effective anisotropic field $\mu_0 H_a = -0.51$ T (for details on the extraction, refer to Section S5 in Supporting **Information**), which has not been reported previously. The negative sign of the effective anisotropic field indicates the magnetization lies in the film plane, while the absolute value determines how large the external field is needed to pull the magnetic moments out of the plane. A zoom-in view of the isothermal magnetization curve (Inset in Figure 1b) reveals zero remanence, indicating the presence of magnetic domains in the material at low field that averages to zero magnetization.

Revealing Room-temperature Magnetism of CFGT Flakes with QMI

Given the small dimension and low mass of exfoliated flakes, a sensitive probe of magnetism capable of room temperature operation is required to investigate thin CFGT flakes. Examples of such probes include magnetic force microscopy (MFM), magnetic optical Kerr effect (MOKE) microscopy⁶, NV scanning probe microscopy^{40, 41}, and more recently magnetic sensing with boron-vacancy in hexagonal boron nitride⁴²⁻⁴⁴. In this work, we employed widefield QMI with NV centers in diamond. Given its ability to detect magnetic field with high-sensitivity and high spatial resolution (diffraction limited), the NV center in diamond realizes a powerful quantum sensor of local magnetic field and hence provides an enabling tool for advancing condensed matter physics and materials science⁴⁵. In particular, the implementation of NV sensing in the form of wide-field magnetic imaging has been applied to study novel electrical flow in graphene⁴⁶, vdW superconductors⁴⁷, as well as 2D magnets both at low-temperatures⁴⁸ as well as at room-temperature³¹. While QMI's diffraction-limited resolution

does not reach the nanoscale resolution offered by scanning probe, it is sufficient for the purpose of this work. Furthermore, QMI is particularly well-positioned for this work because of the ease of operation for high throughput measurement, and the ability to readily detect both in-plane and out-of-plane magnetization. Hence, QMI provides a highly suitable tool for our investigation.

The setup of QMI is described previously³¹ and summarized in Figure 1c. An antenna for delivering microwave (MW) necessary for NV measurement is fabricated on the diamond. We exfoliated CFGT flakes on diamond containing a near-surface NV ensemble. A primary limitation of CFGT is its air sensitivity. Most of vdW magnets degrade in air, though in the recent time certain materials have emerged that demonstrate long-term stability in air^{49, 50}. While air sensitivity of CFGT itself has not been characterized, one can gain insight from the study of a closely-related material Fe₃GeTe₂, which shows insignificant change in magnetic property in 8-layer up to 20 minutes in air³⁸. Assuming similar trend in CFGT, a viable way to protect thin CFGT flakes in air is to deposit protective layer upon them, if the exposure time to air prior to deposition is on the order of minutes or less. We evaporated a thin layer of Al (~5 nm) immediately after exfoliation to protect the flakes from oxidation, with the amount of time between exfoliation and pumping down the sample space of the evaporator to be less than three minutes. As in Ref. ³¹, optically detected magnetic resonance (ODMR) was performed with a camera to image the stray magnetic field generated by CFGT flakes. We adopted the configuration where an out-of-plane (z-direction) bias field B_0 is applied, which enables us to image the distribution of the out-of-plane component of the stray field $B_z(x,y)$.³¹

To help inform what kind of pattern of stray-field distribution one anticipates to observe, we show the simulated $B_z(x,y)$ generated by a square magnetic structure with a uniform out-of-plane (**Figure 2a**) and in-plane 2D magnetization (**Figure 2b**). We note that in each case, stray field with vertical component is generated at a plane above the magnet. The former generates a $B_z(x,y)$ that switches sign at the boundary, where the latter generates a dipole-like pattern that is antisymmetric along the magnetization direction. In **Figures 2c**-h, we show images of experimentally measured stray field distribution of several flakes. Thickness of flakes was measured with atomic force microscopy (AFM) and is 15.7(3) nm (16 layers) for **Figures 2c**, f, 25.6(2) nm (26 layers) for **Figures 2d**, g, and 28.6(3) (29 layers) for **Figures 2e**, h. Thickness is 56.5(6) nm (58 layers) for **Figure 2i**. In **Figures 2c**-e, we show $B_z(x,y)$ with an out-of-plane bias field $B_0 \sim 30$ mT. In each case, we observed $B_z(x,y)$ that has similar

topology to the one shown in **Figure 2**a, indicating that magnetization is directed out-ofplane. We then lowered the bias field to $B_0\sim3$ mT. If the flakes were paramagnetic, the stray field would merely change in amplitude but not topology. Instead, Figures 2h-f show that the stray field undergoes a dramatic change in topology and now manifests spatially-varying pattern, revealing textures in magnetization. This demonstrates ferromagnetic ordering in the flakes at room temperature. The presence of magnetic textures is consistent with the expectation of domains at small out-of-plane field, inferred from bulk magnetization measurement that shows zero remanence and easy-plane anisotropy; magnetic textures may also arise due to steps on the flake surface, but it appears unlikely given the topography of these flakes is mostly uniform (Supporting Information Fig. S3). In **Figure 2**i, we show the stray field of another flake at bias field ~3 mT, which also displays stray field texture, demonstrating that room-temperature ferromagnetism is ubiquitous among CFGT flakes.

Thickness-dependent T_c

We then measured T_c of various flakes shown in **Figure 2**. We employed simultaneous magnetometry-thermometry as described in Ref. ³¹. Heating was provided by a resistive heater, and ODMR imaging provides both B_z and temperature T of the sample. An out-ofplane bias field ~3 mT was used. Because of the presence of domains, we adopted a statistical technique to extract T_c^{51} . For each flake, we select a region-of-interest (ROI) in the neighborhood of the flake, and compute the variance $\Delta B_{ROI}^2 = \langle (B_z - \langle B_z \rangle)^2 \rangle$, where $\langle ... \rangle$ denotes average over the ROI. Below T_c , the presence of stray field texture is captured in the variance, and hence one expects the variance to drop to zero at T_c as temperature is raised, and remains zero beyond T_c . Since fluctuations in measurement can also contribute to variance, we also select a background region in the vicinity of the ROI, and compute the background variance $\Delta B_{\rm BG}^2$. We then compute the normalized variance $\Delta B^2 = \Delta B_{\rm ROI}^2 - \Delta B_{\rm BG}^2$ which provides a proxy for magnetic ordering. In **Figures 3**a-c, ΔB^2 vs T is shown for the three flakes corresponding to Figures 2c-h. In general, we observe ΔB^2 decreases gradually as T increases, and then become flat and vanishingly small above a cutoff temperature, consistent with the expectation of a phase transition leading to the disappearance of ferromagnetic order. A fit to the power-law behavior $v_0+a(1-T/T_c)^{\beta}$ enables the extraction of T_c . We obtain $T_c=309.8(7)$ K, 321(2) K, and 319(2) K for the 16, 26, and 29 layer flakes respectively.

We note that CFGT is ferromagnetic at above room temperature both in the bulk form and in thin flakes down to 16 layers. Furthermore, the Fe₅GeTe₂ family of materials is thermally

stable to temperatures well-above those used during standard exfoliation processes³². Hence, our result adds to the small portfolio of thin (<20 nm) 2D magnets at or above room-temperature created from exfoliation of a single crystal that is magnetic in the bulk and thermally stable within typical temperature range employed in fabrication, with the only other such material being the recently reported Fe₃GaTe₂ ²⁸. The smallest flake thickness probed in this work was constrained by the flakes available in the vicinity of the stripline; in the future, even thinner flakes could be studied by first preparing them on a separate substrate, and then transferring them⁵² near a stripline on a diamond. Nevertheless, the sub-20 nm thickness for which we have observed above-room-temperature ferromagnetism enters the regime where practical spintronic devices can be created. For example, spin-torque oscillator has been fabricated from 17 nm thick yittrium iron garnet⁵³, while highly efficient spin-orbit-torque (SOT) switching has been demonstrated for ~15-20 nm thick Fe₃GeTe₂¹³. Hence, our results pave the way for the development of practical devices based on 2D magnets operational at room-temperature.

For the thicker flake shown in Figure 2i (thickness ~56 nm corresponding to 58 layers), we observe nonhomogeneous temperature-dependent trends in different regions. For example, the region shown in **Figure 3**d is well described by a single power-law behavior with T_c =325.9(3) K, while **Figure 3**e displays a bimodal behavior whose fit requires a superposition of two power-law terms of the form $y_0+a(1-T/T_c)^{\beta}$, giving rise to two transition temperatures ~316 and ~332 K. Another intriguing behavior is observed in the vicinity of the crack indicated in the ROI of Figure 3f. In Figure 2i, a large stray field is observed in the same region, which in fact persists to the highest temperature explored in this work. In **Figure 3**f, we plot the average stray field of this ROI in the vicinity of the crack. For comparison, we also plot the average stray field of a background indicated in the inset, which is nearly zero across all temperatures as expected. However, significant stray field associated with this ROI is observed up to \sim 350 K, indicating magnetization persists up to this temperature. As observed from AFM image (Figure S3, Supporting Information), this flake has several folds and faults. It is reasonable to expect that large and complex strain environment exists within this flake, leading to widely varied transition behavior. The bimodal behavior is consistent with the existence of two phase transitions. While we do not have a definitive explanation for what is the cause of this double phase transition, we do point out that multiple phase transitions and the corresponding multimodal M vs T (which our $(\Delta B)^2$ vs T measurement provide a proxy as) is known in literature, e.g. in bilayer La_{1.4}Sr_{1.6}Mn₂O₇ ⁵⁴ and

even in van der Waals magnet CrI₃ ^{55, 56}. In the work Ref. ⁵⁵, three transitions were observed which are attributed to an interplay of structural and magnetic transitions. Ref. ⁵⁶ observed that in addition to a transition attributed as the standard ferromagnetic transition, a satellite transition also exists at a lower temperature and is proposed to be a crossover from pinning to depinning of magnetic domain walls. Both appear to be possible scenario. In particular, from the AFM topography, we observe there are some structural faults in the vicinity of the region of Fig. 3e, and hence it is possible that structural evolution and/or pinning-depinning behaviors with respect to temperature change may be different compared to other regions.

Monte Carlo Simulations of CFGT Monolayer Using *ab initio* Effective Spin Hamiltonian

To investigate T_c in CFGT monolayer, we employed Monte Carlo simulation using *ab initio* effective spin Hamiltonian. The classical effective low-energy spin Hamiltonian^{57, 58} describing the magnetic states at relevant experimental energy scales

$$H = -\frac{1}{2} \sum_{i,j} \mathbf{S}_{i} \mathbf{J}_{ij} \mathbf{S}_{j} - K \sum_{i} (\mathbf{S}_{i} \cdot \hat{\mathbf{z}})^{2} - \mu_{S} \sum_{i} \mathbf{S}_{i} \cdot \mathbf{B},$$
 (1)

is constructed *ab initio* ⁵⁷ using using noncollinear density functional theory (DFT) calculations. Here, \mathbf{S}_i are unit vectors; \mathbf{J}_{ij} is 3×3 tensor^{58, 59} describing isotropic nearest-neighbor and beyond (as denoted by i, j) exchange interaction, $J_{ij} = \frac{1}{3} \operatorname{Tr} \mathbf{J}_{ij}$; the magnitude of the easy-plane anisotropy is specified by K; and \mathbf{B} is an external magnetic field. Table 1 provides *ab initio* extracted J_{ij} parameters between atoms of CFGT units cell depicted in **Figure 4**a. We also compute the out-of-plane anisotropy, $A = E_{\perp} - E_{\parallel}$, where E_{\perp} and E_{\parallel} are ground state energies for atomic magnetic moments aligned out-of-plane or in-plane, respectively, for both FGT and CFGT monolayers. Such anisotropy is $A = -1.5 \ \mu\text{eV/Fe-atom}$ for FGT and $A = 2 \ \mu\text{eV/Fe-atom}$ for CFGT monolayer. Thus, Co-substitution switches easy-axis anisotropy of FGT to easy-plane anisotropy of CFGT, as encoded by the second term in **Equation 1**. These values are in good agreement with the previous DFT calculations³³. As both 20% and 28% Co-substituted FGT host easy-plane anisotropy, we extract J_{ij} and K parameters in **Equation 1** for 20% Co-substituted FGT to avoid computational expense due to large number of atoms in the supercell. Additional details can be found in **Supporting Information Section S1**.

At T=0, the calculated ground state of CFGT monolayer is an easy-plane ferromagnet, which becomes magnetized out-of-plane with a perpendicular external field at 40 mT. Normalized magnetization m/m_s vs T is shown in **Figure 4**b. A fit to $y_0+a(1-T/T_c)^{\beta}$ yields T_c =271.6(9) K

and β =0.340(6) (see **Section S2** in **Supporting Information** for details of the fit). We note that Mermin-Wagner-Hohenberg theorem⁶⁰ and Berezinskii-Kosterlitz-Thouless scenario⁶¹, which forbid long-range in-plane magnetic order, apply to a purely two-dimensional plane of magnetic atoms with short-range interaction, and hence do not pertain to monolayer CFGT which consists of two atomic planes of magnetic atoms with strong exchange interactions between atoms in the different planes (Table 1) that is comparable to exchange interaction between atoms in the same plane⁶¹. Hence, the existence of a ground state with in-plane long-range magnetic order is reasonable in CFGT monolayer. Our result shows that easy-plane anisotropy persists from the bulk to the monolayer limit. In magnetic memory applications, vertical anisotropy is generally desired given its faster switching, hence CFGT's nature as an easy-plane magnet is a limitation in regards to high-speed operation.

We can compare the T_c of CFGT to the result of pure FGT (lattice structure shown in **Figure** 4a, interaction parameters shown in **Table 2**) where we extracted $T_c = 281.0(5)$ K (**Figure 4**b). This is in contrast to experiments which find T_c to be higher for Co-substituted materials in both bulk crystal (\sim 330 K in CFGT from both Ref. ³³ and this work vs \sim 310K in FGT ³⁰) and in thin flakes (310 K in 16 layers CFGT vs 280-300 K in 12-20 layer flakes $^{30,\,31}$). This is likely due to a preferential site-substitution of cobalt atoms that reduces the magnetic fluctuations on the Fe1 sublattice, bringing the magnetism into greater unity ^{30, 32, 33}. Underlying this higher T_c may also be a change in total transition metal content, specifically a reduced magnetic vacancy concentration. Thus, the experimental CFGT crystals and flakes have a higher T_c than the parent material, but the exact microscopic reason for this remains unknown. From a theoretical perspective, energetics from previous DFT calculations imply that CFGT would have a suppressed T_c relative to the parent material 33 . However, those DFT calculations are on idealized structures and do not take vacancies into account, which seemingly highlights the importance of the disorder effects in these materials. In this work, simulation on monolayer CFGT and FGT also find the same trends, with vacancy-free FGT having a higher theoretical T_c in the monolayer than does CFGT. Importantly, though, these calculations reveal that long-range ferromagnetic order with easy-plane anisotropy can be a stable ground state in this system. Furthermore, we note that similar Monte Carlo calculations for CrI₃, CrBr₃, and CrGeTe₃ have yielded monolayer T_c of 69, 39, and 65 K, which have reasonably good agreement (to within 25 K) with experimental values of 45, 34, and 45 K respectively⁶², and show the same qualitative order in terms of which material has higher/lower T_c . Hence, while the simulations reported here are idealized calculations in

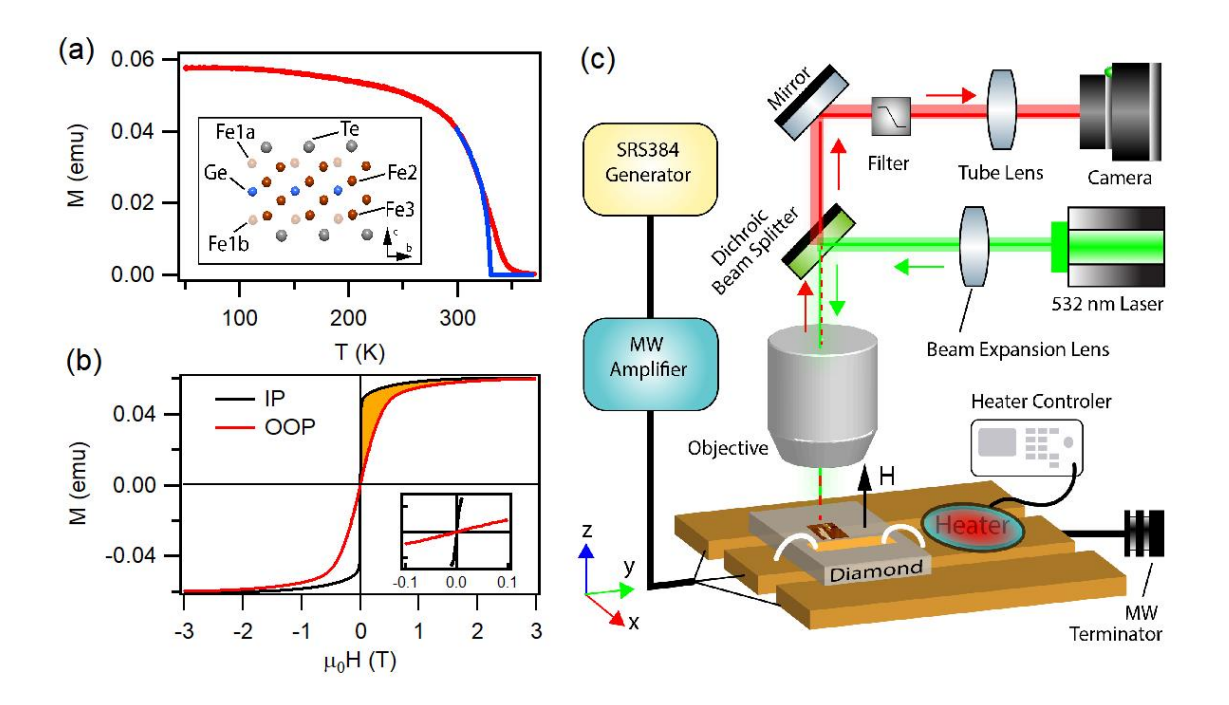
comparison to the complex experimental systems, the qualitative trends reported by the simulations demonstrate that high $T_{\rm c}$ not too far below room temperature may be expected for monolayer CFGT materials, pointing tot he value of further experimental investigation of the materials in the monolayer limit. On the theoretical side, future investigations are needed to understand how the various disorder effects controls the properties in this material.

In Figure 4c, we plot T_c from experimental data as well as from the monolayer calculation to display the trend of thickness dependence. While the calculated monolayer T_c for CFGT is below room temperature, it is in fact not too far from room temperature and even higher than freezer temperature (255 K). Hence, a monolayer with this T_c can readily operate outside of a cryostat when cooled with a thermoelectric cooler (TEC). T_c could be further enhanced via micropatterning⁶³, strain engineering⁶⁴, or via proximity effect^{65,66}, all of which have demonstrated >30 K enhancement in other 2D magnets. Hence, our result points to the prospect of room-temperature or nearly-room-temperature device involving monolayer CFGT, where at most a moderate cooling (e.g. via TEC) that is compatible with a practical working environment is sufficient to ensure operation of the device, and hence the value of future works that further investigate CFGT in the monolayer limit.

CONCLUSION

In conclusion, we have studied exfoliated flakes of CFGT via QMI. We have observed above-room-temperature ferromagnetism in flakes as thin as 16 nm, with T_c ranging from ~310 K in the thinnest flake studied to ~330 K in the bulk. Our results add to the portfolio of thin 2D magnets at above room-temperature created from exfoliation of robust crystals. These results show that CFGT provides a suitable material platform for fabricating high quality devices. Via atomistic *ab initio* calculation, we have obtained a T_c ~270 K in CFGT monolayer. This work establishes CFGT as a platform for high-quality 2D magnetic devices with high Curie temperature, and therefore opens up a number of important directions in the field of 2D magnets. First, our results point to the possibility of monolayer device capable of operation outside of a cryostat requiring only moderate cooling (e.g. via TEC) as well as engineering room-temperature T_c in monolayer via strain, micro-patterning, or proximity effect. Second, even without going into monolayer, our results show that room-temperature 2D magnet now enters the thickness regime in which practical devices can be made and that can take advantage of the unique properties of vdW materials. For example, excellent interface resulting from atomically smooth flat surface, which is a characteristic of vdW materials, can

lead to highly-efficient SOT switching, even for flakes ~15-20 nm thick. ¹³ Hence, our results pave the way for creating energy-efficient spintronic devices at room-temperature with thin CFGT flakes, such as SOT-magnetic random-access memory and spin-torque oscillator. Lastly, our work also opens up the direction towards engineering novel magnetic phases in thin 2D magnet at or near room-temperature, e.g. non-collinear texture or skyrmion via proximity effect or twist engineering ^{8-10, 67}.



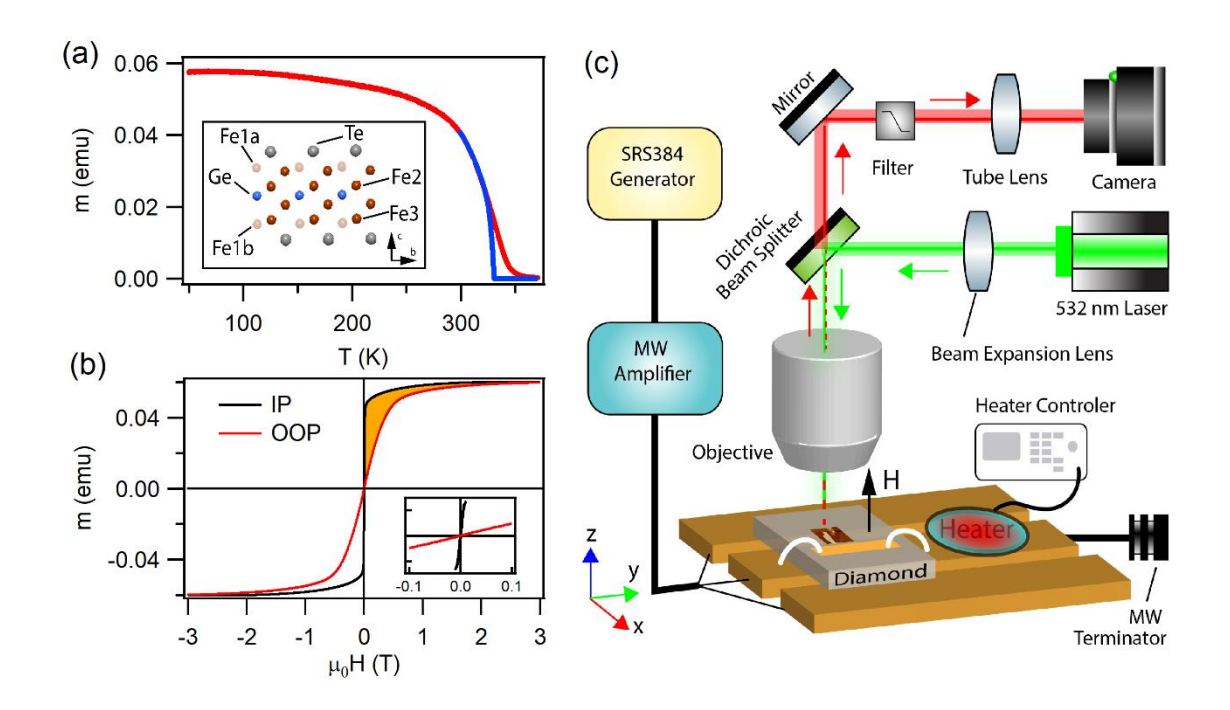


Figure 1. (a) Temperature-dependent magnetization measurement M vs T for bulk CFGT crystal. A fit near the critical region (blue curve) extracts T_c =328 K (see Section S4 in Supporting Information for details of the fit). The inset shows the lattice structure of CFGT; a single layer is shown. Fe1a and Fe1b correspond to a split site that allows for local atomic order and disorder; Co-substitution of these sites is energetically favorable compared to Fe2 or Fe3 sites. For simplicity, the associated split site of Ge is not illustrated. (b) Isothermal magnetization measurement M vs H measurement at room-temperature for in-plane (IP) and out-of-plane (OOP) H, showing saturation behavior and easy-plane anisotropy. For OOP data, the horizontal axis takes into account the demagnetization correction (see Section S5 in Supporting Information). Inset: zoom-in bulk in-plane measurement shows zero remanence, and hence the presence of domains. (c) Schematics of QMI.

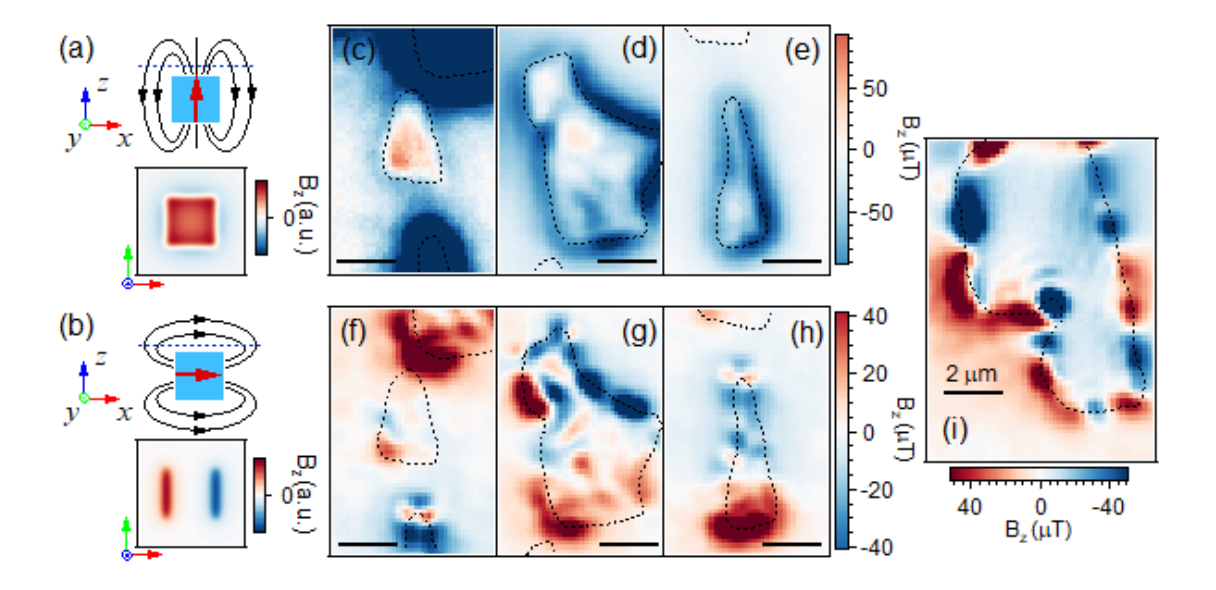


Figure 2. Quantum magnetic imaging of CFGT flakes. a) and b): Simulated distribution of vertical stray field B_z for uniform a) out-of-plane (pointing along z) and b) in-plane (pointing along x) magnetization. Here, one assumes a 2D 1 μm × 1 μm square of magnetization, and stray field is simulated at a stand-off distance d=100 nm. Images are convolved with a point spread function corresponding to 600 nm optical resolution of the experimental setup. c)-e) Experimental stray field of CFGT flakes at room temperature with an applied vertical bias field (along z-direction) \sim 30 mT. These images have similar topology to a), demonstrating that magnetization is aligned along the vertical (z-) direction. f)-h): Measurement of the same flakes corresponding to c-e respectively, but with a smaller vertical bias field ~3 mT. Here, we see a stray field texture, characterized by multiple changes of sign in a flake, develops that reveals underlying domains. Magnetizations that get oriented along the bias field at high field and forms domains at low field demonstrate that these flakes have ferromagnetic order. Thickness of flakes are 15.7(3) nm (16 layers) for c, f, 25.6(2) nm (26 layers) for d, g, and 28.6(3) nm (29 layers) for e, h. i) Measurement of a 56.5(6) nm thick (58 layers) flake under the same condition as f-h. All experimental images are shown to the same scale; all scale bars are for 2 µm.

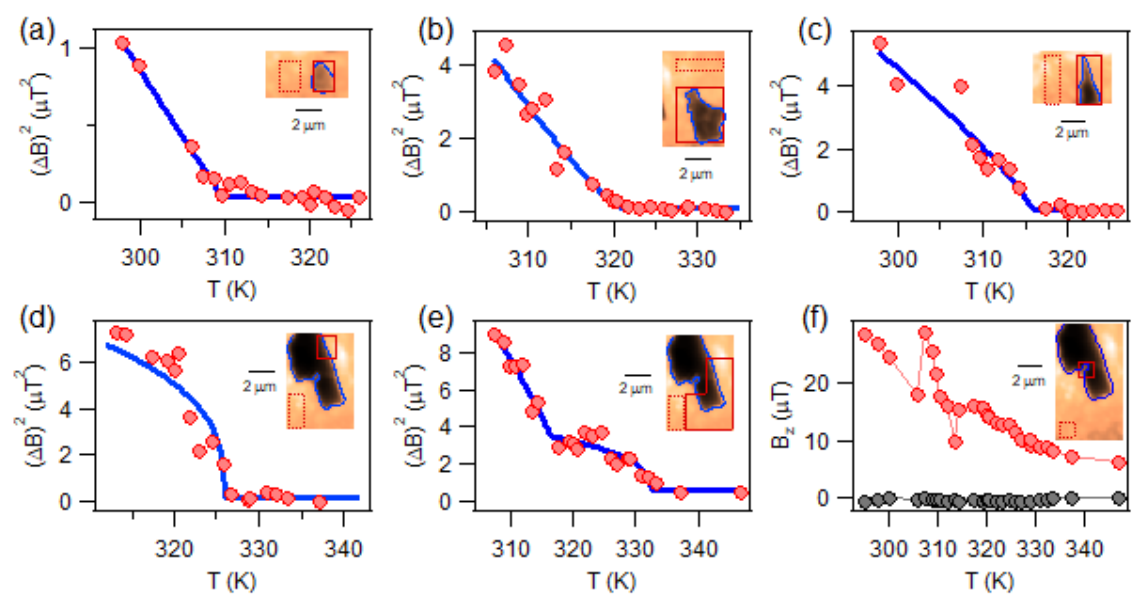


Figure 3. Temperature-dependent measurement. Panels (a-e) show normalized variance $\Delta B^2 = \Delta B_{\rm ROI}^2 - \Delta B_{\rm BG}^2$ as a function of temperature T, where $\Delta B_{\rm A}^2 = \langle (B_z - \langle B_z \rangle)^2 \rangle$ with A corresponding to the area over which statistical averaging $\langle ... \rangle$ is performed. In the inset of each panel, an optical image of the flake is shown, together with the region-of-interest (ROI) in the neighborhood of the flake shown as solid red rectangle, and background (BG) shown as dashed red rectangle. Flake thickness is (a) 15.7 nm (6 layers), (b) 25.6nm (26 layers), (c) 28.6 nm (29 layers), and (d-e) 56.5 nm (58 layers). Experimental data of ΔB^2 vs T is shown in red circles. Data is fit to power-law behavior $y_0 + A(1 - T/T_c)^\beta$, except for (e) which is fit to a superposition of two such terms. Fit is shown in blue curve. Extracted T_c is (a) 309.8(7) K, (b) 321(2) K, (c) 319(2) K, and (d) 325.9(3) K. For (e), two temperatures ~316 and ~322 K are extracted. (f) Average stray field of the ROI (red) and average stray field of the BG (black circles) vs T.

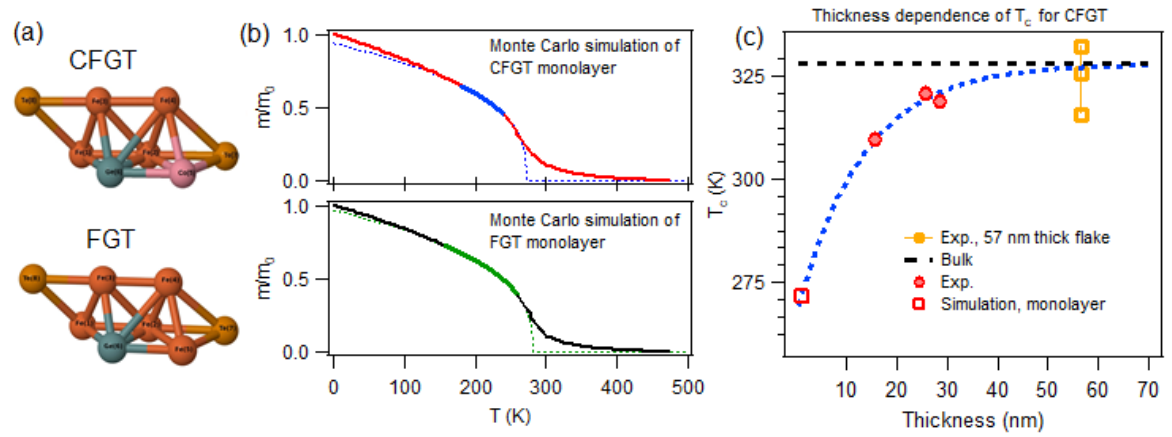


Figure 4. Monte Carlo simulation of CFGT and FGT monolayer. (a) Lattice considered in the calculation for CFGT (top) and FGT (bottom). Exchange couplings between spins are listed in Table 1 (CFGT) and Table 2 (FGT). (b) Average magnetization m vs temperature T, normalized by magnetization m_0 at T=0. Simulation results are shown for CFGT (red, upper panel) and FGT (black, bottom panel) A fit to power-law $y_0+A(1-T/T_c)^\beta$ near the phase transition extracts T_c =271.6(9) K and β =0.340(6) for CFGT, and T_c =281.0(5) K and β =0.352(3) for FGT. Blue (green) solid curve in the upper (bottom) panel is the fitted model across the fitted temperature range for CFGT (FGT); blue (green) dashed curve in the upper (bottom) panel is the fitted model across the entire temperature range for CFGT (FGT). (c) Experimental T_c vs thickness for the 16-29 nm thick flakes (red circles) and 57 nm thick flake (orange), and CFGT monolayer value from calculation (red open square). Black dashed line is bulk value 328 K. Blue dashed curve is a guide to the eye.

Table 1. Values of exchange coupling J_{ij} between sites as labeled in Figure 4a for CFGT.

System	J_{ij} (meV)
Fe(1)- $Fe(2)$	54.1539
Fe(1)- $Fe(3)$	33.5254
Fe(1)- $Fe(4)$	-0.7548
Fe(2)- $Fe(3)$	2.1669
Fe(2)- $Fe(4)$	26.9815
Fe(2)- $Co(5)$	1.9647
Fe(3)- $Fe(4)$	28.4089
Fe(4)- $Co(5)$	7.6406

Table 2. Values of exchange coupling J_{ij} between sites as labeled in Figure 4a for FGT.

	8
System	J_{ij} (meV)
Fe(1)-Fe(2)	42.2640
Fe(1)- $Fe(3)$	32.5760
Fe(1)- $Fe(4)$	0.0773
Fe(2)- $Fe(3)$	4.7758
Fe(2)- $Fe(4)$	21.1770
Fe(2)-Fe(5)	9.1585
Fe(3)- $Fe(4)$	21.2840
Fe(4)-Fe(5)	8.7697

ASSOCIATED CONTENT

Supporting Information.

- -Phase transition of monolayer CFGT and FGT from classical Monte Carlo simulations using ab initio effective spin Hamiltonian;
- -Extracting T_c and critical exponent of data from Monte Carlo simulation of CFGT monolayer;
- -Monte Carlo simulation results for CFGT and FGT;
- -Extracting T_c of bulk crystal from magnetometry data;
- -Extracting anisotropy constant H_a of bulk crystal from magnetometry data;
- -Atomic force microscopy image of thick CFGT flake;
- -Monolayer CFGT simulation-discussion of universality class and evasion of Mermin-Wagner-Hohenberg and Berezinskii-Kosterlitz-Thouless scenarios.

AUTHOR INFORMATION

Corresponding Author

* Email: mku@udel.edu

Author Contributions

The manuscript was written through contributions of all authors. All authors have given approval to the final version of the manuscript. †These authors contributed equally.

ACKNOWLEDGEMENTS

This research was partially supported by NSF through the University of Delaware Materials Research Science and Engineering Center DMR-2011824 Seed Award program. Bulk crystal synthesis and characterization (AFM, MAM) were supported by the U. S. Department of Energy, Office of Science, Basic Energy Sciences, Materials Sciences and Engineering Division. KD, VMLDPG, MBJ, BKN, and JQX were supported by NSF through the University of Delaware Materials Research Science and Engineering Center, DMR-2011824. D.J. acknowledges support from a seed grant from the National Science Foundation (NSF) supported University of Pennsylvania Materials Research Science and Engineering Center (MRSEC) (DMR-1720530). H.Z. was partially supported by the Vagelos Institute of Energy Science and Technology graduate fellowship. ZJC and KL were supported by the NSF (DMR-2005108).

REFERENCES

- (1) Huang, B.; Clark, G.; Navarro-Moratalla, E.; Klein, D. R.; Cheng, R.; Seyler, K. L.; Zhong, D.; Schmidgall, E.; McGuire, M. A.; Cobden, D. H.; Yao, W.; Xiao, D.; Jarillo-Herrero, P.; Xu, X., Layer-dependent Ferromagnetism in a van der Waals Crystal Down to the Monolayer Limit. *Nature* **2017**, *546*, 270-273.
- (2) Gong, C.; Li, L.; Li, Z.; Ji, H.; Stern, A.; Xia, Y.; Cao, T.; Bao, W.; Wang, C.; Wang, Y.; Qiu, Z. Q.; Cava, R. J.; Louie, S. G.; Xia, J.; Zhang, X., Discovery of Intrinsic Ferromagnetism in Two-dimensional van der Waals Crystals. *Nature* **2017**, *546*, 265-269. (3) Gibertini, M.; Koperski, M.; Morpurgo, A. F.; Novoselov, K. S., Magnetic 2D Materials and Heterostructures. *Nat Nanotechnol* **2019**, *14*, 408-419.
- (4) Burch, K. S.; Mandrus, D.; Park, J. G., Magnetism in Two-dimensional van der Waals Materials. *Nature* **2018**, *563*, 47-52.
- (5) Gong, C.; Zhang, X., Two-dimensional Magnetic Crystals and Emergent Heterostructure Devices. *Science* **2019**, *363*, eaav4450.
- (6) Huang, B.; McGuire, M. A.; May, A. F.; Xiao, D.; Jarillo-Herrero, P.; Xu, X., Emergent Phenomena and Proximity Effects in Two-dimensional Magnets and Heterostructures. *Nat Mater* **2020**, *19*, 1276-1289.
- (7) Bedoya-Pinto, A.; Ji, J.-R.; Pandeya, A. K.; Gargiani, P.; Valvidares, M.; Sessi, P.; Taylor, J. M.; Radu, F.; Chang, K.; Parkin, S. S., Intrinsic 2D-XY Ferromagnetism in a Van Der Waals Monolayer. *Science* **2021**, *374*, 616-620.
- (8) Song, T.; Sun, Q.-C.; Anderson, E.; Wang, C.; Qian, J.; Taniguchi, T.; Watanabe, K.; McGuire, M. A.; Stöhr, R.; Xiao, D., Direct Visualization of Magnetic Domains and Moiré Magnetism in Twisted 2D Magnets. *Science* **2021**, *374*, 1140-1144.
- (9) Xie, H.; Luo, X.; Ye, G.; Ye, Z.; Ge, H.; Sung, S. H.; Rennich, E.; Yan, S.; Fu, Y.; Tian, S.; Lei, H.; Hovden, R.; Sun, K.; He, R.; Zhao, L., Twist Engineering of the Two-dimensional Magnetism in Double Bilayer Chromium Triiodide Homostructures. *Nature Physics* **2021**, *18*, 30-36.
- (10) Xie, H.; Luo, X.; Ye, Z.; Ye, G.; Ge, H.; Yan, S.; Fu, Y.; Tian, S.; Lei, H.; Sun, K., Evidence of Noncollinear Spin Texture in Magnetic Moiré Superlattices. *arXiv* preprint *arXiv*:2204.01636 **2022**.
- (11) MacNeill, D.; Hou, J. T.; Klein, D. R.; Zhang, P.; Jarillo-Herrero, P.; Liu, L., Gigahertz Frequency Antiferromagnetic Resonance and Strong Magnon-Magnon Coupling in the Layered Crystal CrCl₃. *Phys Rev Lett* **2019**, *123*, 047204.
- (12) Sklenar, J.; Zhang, W., Self-Hybridization and Tunable Magnon-Magnon Coupling in van der Waals Synthetic Magnets. *Physical Review Applied* **2021**, *15*, 044008.
- (13) Alghamdi, M.; Lohmann, M.; Li, J.; Jothi, P. R.; Shao, Q.; Aldosary, M.; Su, T.; Fokwa, B. P. T.; Shi, J., Highly Efficient Spin-Orbit Torque and Switching of Layered Ferromagnet Fe₃GeTe₂. *Nano Lett* **2019**, *19*, 4400-4405.
- (14) Awschalom, D. D.; Du, C. R.; He, R.; Heremans, F. J.; Hoffmann, A.; Hou, J.; Kurebayashi, H.; Li, Y.; Liu, L.; Novosad, V.; Sklenar, J.; Sullivan, S. E.; Sun, D.; Tang, H.; Tyberkevych, V.; Trevillian, C.; Tsen, A. W.; Weiss, L. R.; Zhang, W.; Zhang, X.; Zhao, L.; Zollitsch, C. W., Quantum Engineering With Hybrid Magnonic Systems and Materials (Invited Paper). *IEEE Transactions on Quantum Engineering* **2021**, *2*, 1-36.
- (15) Chumak, A. V.; Kabos, P.; Wu, M.; Abert, C.; Adelmann, C.; Adeyeye, A. O.; Akerman, J.; Aliev, F. G.; Anane, A.; Awad, A.; Back, C. H.; Barman, A.; Bauer, G. E. W.; Becherer, M.; Beginin, E. N.; Bittencourt, V. A. S. V.; Blanter, Y. M.; Bortolotti, P.; Boventer, I.; Bozhko, D. A.; Bunyaev, S. A.; Carmiggelt, J. J.; Cheenikundil, R. R.; Ciubotaru, F.; Cotofana, S.; Csaba, G.; Dobrovolskiy, O. V.; Dubs, C.; Elyasi, M.; Fripp, K. G.; Fulara, H.; Golovchanskiy, I. A.; Gonzalez-Ballestero, C.; Graczyk, P.; Grundler, D.; Gruszecki, P.; Gubbiotti, G.; Guslienko, K.; Haldar, A.; Hamdioui, S.; Hertel, R.; Hillebrands, B.; Hioki, T.; Houshang, A.; Hu, C. M.; Huebl, H.; Huth, M.; Iacocca, E.; Jungfleisch, M. B.; Kakazei, G. N.; Khitun, A.; Khymyn, R.; Kikkawa, T.; Klaui, M.; Klein, O.; Klos, J. W.; Knauer, S.;

- Koraltan, S.; Kostylev, M.; Krawczyk, M.; Krivorotov, I. N.; Kruglyak, V. V.; Lachance-Quirion, D.; Ladak, S.; Lebrun, R.; Li, Y.; Lindner, M.; Macedo, R.; Mayr, S.; Melkov, G. A.; Mieszczak, S.; Nakamura, Y.; Nembach, H. T.; Nikitin, A. A.; Nikitov, S. A.; Novosad, V.; Otalora, J. A.; Otani, Y.; Papp, A.; Pigeau, B.; Pirro, P.; Porod, W.; Porrati, F.; Qin, H.; Rana, B.; Reimann, T.; Riente, F.; Romero-Isart, O.; Ross, A.; Sadovnikov, A. V.; Safin, A. R.; Saitoh, E.; Schmidt, G.; Schultheiss, H.; Schultheiss, K.; Serga, A. A.; Sharma, S.; Shaw, J. M.; Suess, D.; Surzhenko, O.; Szulc, K.; Taniguchi, T.; Urbanek, M.; Usami, K.; Ustinov, A. B.; van der Sar, T.; van Dijken, S.; Vasyuchka, V. I.; Verba, R.; Kusminskiy, S. V.; Wang, Q.; Weides, M.; Weiler, M.; Wintz, S.; Wolski, S. P.; Zhang, X., Advances in Magnetics Roadmap on Spin-Wave Computing. IEEE Transactions on Magnetics 2022, 58, 1-72. (16) Fei, Z.; Huang, B.; Malinowski, P.; Wang, W.; Song, T.; Sanchez, J.; Yao, W.; Xiao, D.; Zhu, X.; May, A. F.; Wu, W.; Cobden, D. H.; Chu, J. H.; Xu, X., Two-dimensional Itinerant Ferromagnetism in Atomically Thin Fe₃GeTe₂. Nat Mater **2018**, 17, 778-782. (17) O'Hara, D. J.; Zhu, T.; Trout, A. H.; Ahmed, A. S.; Luo, Y. K.; Lee, C. H.; Brenner, M. R.; Rajan, S.; Gupta, J. A.; McComb, D. W.; Kawakami, R. K., Room Temperature Intrinsic Ferromagnetism in Epitaxial Manganese Selenide Films in the Monolayer Limit. Nano Lett
- (18) Li, J.; Zhao, B.; Chen, P.; Wu, R.; Li, B.; Xia, Q.; Guo, G.; Luo, J.; Zang, K.; Zhang, Z.; Ma, H.; Sun, G.; Duan, X.; Duan, X., Synthesis of Ultrathin Metallic MTe₂ (M = V, Nb, Ta) Single-Crystalline Nanoplates. *Adv Mater* **2018**, *30*, e1801043.

2018, 18, 3125-3131.

- (19) Yu, W.; Li, J.; Herng, T. S.; Wang, Z.; Zhao, X.; Chi, X.; Fu, W.; Abdelwahab, I.; Zhou, J.; Dan, J.; Chen, Z.; Chen, Z.; Li, Z.; Lu, J.; Pennycook, S. J.; Feng, Y. P.; Ding, J.; Loh, K. P., Chemically Exfoliated VSe₂ Monolayers with Room-Temperature Ferromagnetism. *Adv Mater* **2019**, *31*, e1903779.
- (20) Wang, H.; Liu, Y.; Wu, P.; Hou, W.; Jiang, Y.; Li, X.; Pandey, C.; Chen, D.; Yang, Q.; Wang, H.; Wei, D.; Lei, N.; Kang, W.; Wen, L.; Nie, T.; Zhao, W.; Wang, K. L., Above Room-Temperature Ferromagnetism in Wafer-Scale Two-Dimensional van der Waals Fe₃GeTe₂ Tailored by a Topological Insulator. *ACS Nano* **2020**, *14*, 10045-10053.
- (21) Ribeiro, M.; Gentile, G.; Marty, A.; Dosenovic, D.; Okuno, H.; Vergnaud, C.; Jacquot, J.-F.; Jalabert, D.; Longo, D.; Ohresser, P.; Hallal, A.; Chshiev, M.; Boulle, O.; Bonell, F.; Jamet, M., Large-scale Epitaxy of Two-dimensional van der Waals Room-temperature Ferromagnet Fe₅GeTe₂. *npj 2D Materials and Applications* **2022**, *6*, 10.
- (22) Deng, Y.; Yu, Y.; Shi, M. Z.; Guo, Z.; Xu, Z.; Wang, J.; Chen, X. H.; Zhang, Y., Quantum Anomalous Hall Effect in Intrinsic Magnetic Topological Insulator MnBi₂Te₄. *Science* **2020**, *367*, 895-900.
- (23) Deng, Y.; Yu, Y.; Song, Y.; Zhang, J.; Wang, N. Z.; Sun, Z.; Yi, Y.; Wu, Y. Z.; Wu, S.; Zhu, J., Gate-tunable Room-temperature Ferromagnetism in Two-dimensional Fe₃GeTe₂. *Nature* **2018**, *563*, 94-99.
- (24) Weber, D.; Trout, A. H.; McComb, D. W.; Goldberger, J. E., Decomposition-Induced Room-Temperature Magnetism of the Na-Intercalated Layered Ferromagnet Fe_(3-x)GeTe₂. *Nano Lett* **2019**, *19*, 5031-5035.
- (25) Freitas, D. C.; Weht, R.; Sulpice, A.; Remenyi, G.; Strobel, P.; Gay, F.; Marcus, J.; Nunez-Regueiro, M., Ferromagnetism in Layered Metastable 1T-CrTe₂. *J Phys Condens Matter* **2015**, *27*, 176002.
- (26) Sun, X.; Li, W.; Wang, X.; Sui, Q.; Zhang, T.; Wang, Z.; Liu, L.; Li, D.; Feng, S.; Zhong, S.; Wang, H.; Bouchiat, V.; Nunez Regueiro, M.; Rougemaille, N.; Coraux, J.; Purbawati, A.; Hadj-Azzem, A.; Wang, Z.; Dong, B.; Wu, X.; Yang, T.; Yu, G.; Wang, B.; Han, Z.; Han, X.; Zhang, Z., Room Temperature Ferromagnetism in Ultra-thin van der Waals Crystals of 1T-CrTe₂. *Nano Research* **2020**, *13*, 3358-3363.
- (27) Wang, X.; Li, D.; Li, Z.; Wu, C.; Che, C. M.; Chen, G.; Cui, X., Ferromagnetism in 2D Vanadium Diselenide. *ACS Nano* **2021**, *15*, 16236-16241.

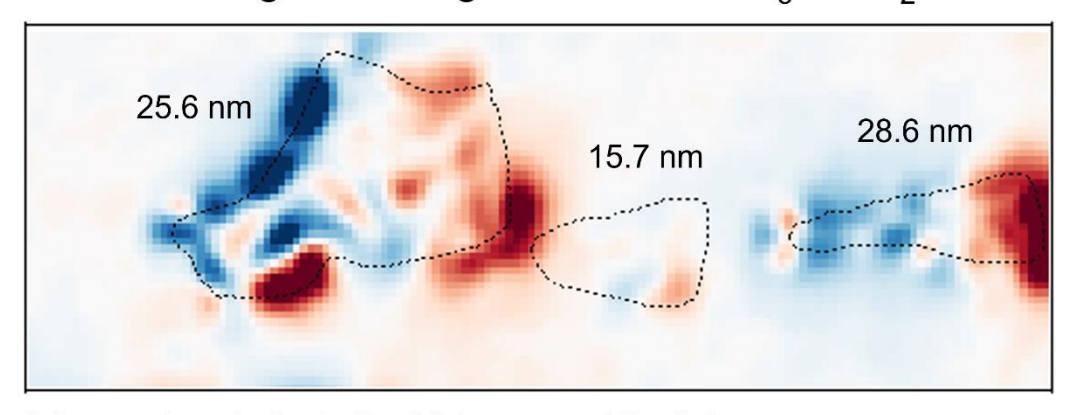
- (28) Zhang, G.; Guo, F.; Wu, H.; Wen, X.; Yang, L.; Jin, W.; Zhang, W.; Chang, H., Aboveroom-temperature Strong Intrinsic Ferromagnetism in 2D van der Waals Fe₃GaTe₂ with Large Perpendicular Magnetic Anisotropy. *Nat Commun* **2022**, *13*, 5067.
- (29) Seo, J.; Kim, D. Y.; An, E. S.; Kim, K.; Kim, G.-Y.; Hwang, S.-Y.; Kim, D. W.; Jang, B. G.; Kim, H.; Eom, G., Nearly Room Temperature Ferromagnetism in a Magnetic Metal-rich van der Waals Metal. *Science advances* **2020**, *6*, eaay8912.
- (30) May, A. F.; Ovchinnikov, D.; Zheng, Q.; Hermann, R.; Calder, S.; Huang, B.; Fei, Z.; Liu, Y.; Xu, X.; McGuire, M. A., Ferromagnetism Near Room Temperature in the Cleavable van der Waals Crystal Fe₅GeTe₂. *ACS Nano* **2019**, *13*, 4436-4442.
- (31) Chen, H.; Asif, S.; Whalen, M.; Támara-Isaza, J.; Luetke, B.; Wang, Y.; Wang, X.; Ayako, M.; Lamsal, S.; May, A. F.; McGuire, M. A.; Chakraborty, C.; Xiao, J. Q.; Ku, M. J. H., Revealing Room Temperature Ferromagnetism in Exfoliated Fe₅GeTe₂ Flakes with Quantum Magnetic Imaging. *2D Materials* **2022**, *9*, 025017.
- (32) May, A. F.; Bridges, C. A.; McGuire, M. A., Physical Properties and Thermal Stability of Fe_{5-x}GeTe₂ Single Crystals. *Physical Review Materials* **2019**, *3*, 104401.
- (33) May, A. F.; Du, M.-H.; Cooper, V. R.; McGuire, M. A., Tuning Magnetic Order in the van der Waals Metal Fe₅GeTe₂ by Cobalt Substitution. *Physical Review Materials* **2020**, *4*, 074008.
- (34) Tian, C.; Pan, F.; Xu, S.; Ai, K.; Xia, T.; Cheng, P., Tunable Magnetic Properties in van der Waals Crystals (Fe_{1-x}Co_x)₅GeTe₂. *Applied Physics Letters* **2020**, *116*, 202402.
- (35) Zhang, H.; Raftrey, D.; Chan, Y.-T.; Shao, Y.-T.; Chen, R.; Chen, X.; Huang, X.; Reichanadter, J. T.; Dong, K.; Susarla, S., Room-temperature Skyrmion Lattice in a Layered Magnet (Fe_{0.5}Co_{0.5})₅GeTe₂. *Science advances* **2022**, *8*, eabm7103.
- (36) Zhang, H.; Shao, Y.-T.; Chen, R.; Chen, X.; Susarla, S.; Raftrey, D.; Reichanadter, J. T.; Caretta, L.; Huang, X.; Settineri, N. S.; Chen, Z.; Zhou, J.; Bourret-Courchesne, E.; Ercius, P.; Yao, J.; Fischer, P.; Neaton, J. B.; Muller, D. A.; Birgeneau, R. J.; Ramesh, R., A room Temperature Polar Magnetic Metal. *Physical Review Materials* **2022**, *6*, 044403.
- (37) Chen, X.; Schierle, E.; He, Y.; Vranas, M.; Freeland, J. W.; McChesney, J. L.; Ramesh, R.; Birgeneau, R. J.; Frano, A., Antiferromagnetic Order in Co-doped Fe₅GeTe₂ Probed by Resonant Magnetic X-ray Scattering. *Physical Review Materials* **2022**, *6*, 094404.
- (38) Tu, Z.; Xie, T.; Lee, Y.; Zhou, J.; Admasu, A. S.; Gong, Y.; Valanoor, N.; Cumings, J.; Cheong, S.-W.; Takeuchi, I.; Cho, K.; Gong, C., Ambient Effect on the Curie Temperatures and Magnetic Domains in Metallic Two-dimensional Magnets. *npj 2D Materials and Applications* **2021**, *5*, 62.
- (39) May, A. F.; Yan, J.; McGuire, M. A., A Practical Guide for Crystal Growth of van der Waals Layered Materials. *Journal of Applied Physics* **2020**, *128*, 051101.
- (40) Thiel, L.; Wang, Z.; Tschudin, M. A.; Rohner, D.; Gutierrez-Lezama, I.; Ubrig, N.; Gibertini, M.; Giannini, E.; Morpurgo, A. F.; Maletinsky, P., Probing Magnetism in 2D Materials at the Nanoscale with Single-spin Microscopy. *Science* **2019**, *364*, 973-976.
- (41) Fabre, F.; Finco, A.; Purbawati, A.; Hadj-Azzem, A.; Rougemaille, N.; Coraux, J.; Philip, I.; Jacques, V., Characterization of Room-temperature In-plane Magnetization in Thin Flakes of CrTe₂ with a Single-spin Magnetometer. *Physical Review Materials* **2021**, *5*, 034008.
- (42) Kumar, P.; Fabre, F.; Durand, A.; Clua-Provost, T.; Li, J.; Edgar, J.; Rougemaille, N.; Coraux, J.; Marie, X.; Renucci, P., Magnetic Imaging with Spin Defects in Hexagonal Boron Nitride. *arXiv preprint arXiv:2207.10477* **2022**.
- (43) Huang, M.; Zhou, J.; Chen, D.; Lu, H.; McLaughlin, N. J.; Li, S.; Alghamdi, M.; Djugba, D.; Shi, J.; Wang, H.; Du, C. R., Wide Field Imaging of van der Waals Ferromagnet Fe₃GeTe₂ by Spin Defects in Hexagonal Boron Nitride. *Nat Commun* **2022**, *13*, 5369.

- (44) Healey, A.; Scholten, S.; Yang, T.; Scott, J.; Abrahams, G.; Robertson, I.; Hou, X.; Guo, Y.; Rahman, S.; Lu, Y., Quantum Microscopy with van der Waals Heterostructures. *Nature Physics* **2022**, 1-5.
- (45) Casola, F.; van der Sar, T.; Yacoby, A., Probing Condensed Matter Physics with Magnetometry Based on Nitrogen-vacancy Centres in Diamond. *Nature Reviews Materials* **2018**, *3*, 1-13.
- (46) Ku, M. J. H.; Zhou, T. X.; Li, Q.; Shin, Y. J.; Shi, J. K.; Burch, C.; Anderson, L. E.; Pierce, A. T.; Xie, Y.; Hamo, A.; Vool, U.; Zhang, H.; Casola, F.; Taniguchi, T.; Watanabe, K.; Fogler, M. M.; Kim, P.; Yacoby, A.; Walsworth, R. L., Imaging Viscous Flow of the Dirac Fluid in Graphene. *Nature* **2020**, *583*, 537-541.
- (47) McLaughlin, N. J.; Wang, H.; Huang, M.; Lee-Wong, E.; Hu, L.; Lu, H.; Yan, G. Q.; Gu, G.; Wu, C.; You, Y. Z.; Du, C. R., Strong Correlation Between Superconductivity and Ferromagnetism in an Fe-Chalcogenide Superconductor. *Nano Lett* **2021**, *21*, 7277-7283.
- (48) Broadway, D. A.; Scholten, S. C.; Tan, C.; Dontschuk, N.; Lillie, S. E.; Johnson, B. C.; Zheng, G.; Wang, Z.; Oganov, A. R.; Tian, S.; Li, C.; Lei, H.; Wang, L.; Hollenberg, L. C. L.; Tetienne, J. P., Imaging Domain Reversal in an Ultrathin Van der Waals Ferromagnet. *Adv Mater* **2020**, *32*, e2003314.
- (49) Son, J.; Son, S.; Park, P.; Kim, M.; Tao, Z.; Oh, J.; Lee, T.; Lee, S.; Kim, J.; Zhang, K.; Cho, K.; Kamiyama, T.; Lee, J. H.; Mak, K. F.; Shan, J.; Kim, M.; Park, J. G.; Lee, J., Air-Stable and Layer-Dependent Ferromagnetism in Atomically Thin van der Waals CrPS(4). *ACS Nano* **2021**, *15*, 16904-16912.
- (50) Su, J.; Wang, M.; Liu, G.; Li, H.; Han, J.; Zhai, T., Air Stable 2D Intrinsic Ferromagnetic Ta₃FeS₆ with Four Months Durability. *Advanced Science* **2020**, *7*, 2001722.
- (51) Nava Antonio, G.; Bertelli, I.; Simon, B. G.; Medapalli, R.; Afanasiev, D.; van der Sar, T., Magnetic Imaging and Statistical Analysis of the Metamagnetic Phase Transition of FeRh with Electron Spins in Diamond. *Journal of Applied Physics* **2021**, *129*, 223904.
- (52) Wang, L.; Meric, I.; Huang, P.; Gao, Q.; Gao, Y.; Tran, H.; Taniguchi, T.; Watanabe, K.; Campos, L.; Muller, D., One-dimensional Electrical Contact to a Two-dimensional Material. *Science* **2013**, *342*, 614-617.
- (53) Zhang, H.; Ku, M. J. H.; Casola, F.; Du, C. H. R.; van der Sar, T.; Onbasli, M. C.; Ross, C. A.; Tserkovnyak, Y.; Yacoby, A.; Walsworth, R. L., Spin-torque Oscillation in a Magnetic Insulator Probed by a Single-spin Sensor. *Physical Review B* **2020**, *102*, 024404.
- (54) Kumar, B.; Tiwari, J. K.; Chauhan, H. C.; Ghosh, S., Multiple Magnetic Phase Transitions with Different Universality Classes in Bilayer La_{1.4}Sr_{1.6} Mn₂O₇ Manganite. *Scientific Reports* **2021**, *11*, 1-17.
- (55) Meseguer-Sánchez, J.; Popescu, C.; García-Muñoz, J. L.; Luetkens, H.; Taniashvili, G.; Navarro-Moratalla, E.; Guguchia, Z.; Santos, E. J., Coexistence of Structural and Magnetic Phases in van der Waals Magnet CrI₃. *Nature communications* **2021**, *12*, 1-7.
- (56) Liu, Y.; Wu, L.; Tong, X.; Li, J.; Tao, J.; Zhu, Y.; Petrovic, C., Thickness-dependent Magnetic Order in CrI₃ Single Crystals. *Scientific Reports* **2019**, *9*, 1-8.
- (57) Riedl, K.; Li, Y.; Valentí, R.; Winter, S. M., Ab Initio Approaches for Low-energy Spin Hamiltonians. *physica status solidi (b)* **2019**, *256*, 1800684.
- (58) Li, X.; Yu, H.; Lou, F.; Feng, J.; Whangbo, M.-H.; Xiang, H., Spin Hamiltonians in Magnets: Theories and Computations. *Molecules* **2021**, *26*, 803.
- (59) Evans, R. F.; Fan, W. J.; Chureemart, P.; Ostler, T. A.; Ellis, M. O.; Chantrell, R. W., Atomistic Spin Model Simulations of Magnetic Nanomaterials. *Journal of Physics: Condensed Matter* **2014**, *26*, 103202.
- (60) Mermin, N. D.; Wagner, H., Absence of Ferromagnetism or Antiferromagnetism in One-or Two-dimensional Isotropic Heisenberg Models. *Physical Review Letters* **1966**, *17*, 1133.

- (61) Olsen, T., Theory and Simulations of Critical Temperatures in CrI₃ and Other 2D Materials: Easy-axis Magnetic Order and Easy-plane Kosterlitz-Thouless Transitions. *MRS Communications* **2019**, *9*, 1142-1150.
- (62) Tiwari, S.; Van de Put, M. L.; Soree, B.; Vandenberghe, W. G., Critical Behavior of the Ferromagnets CrI₃, CrBr₃, and CrGeTe₃ and the Antiferromagnet FeCl₂: a Detailed First-principles Study. *Physical Review B* **2021**, *103*, 014432.
- (63) Li, Q.; Yang, M.; Gong, C.; Chopdekar, R. V.; N'Diaye, A. T.; Turner, J.; Chen, G.; Scholl, A.; Shafer, P.; Arenholz, E.; Schmid, A. K.; Wang, S.; Liu, K.; Gao, N.; Admasu, A. S.; Cheong, S. W.; Hwang, C.; Li, J.; Wang, F.; Zhang, X.; Qiu, Z., Patterning-Induced Ferromagnetism of Fe₃GeTe₂ van der Waals Materials beyond Room Temperature. *Nano Lett* **2018**, *18*, 5974-5980.
- (64) Zhong, J.; Wang, M.; Liu, T.; Zhao, Y.; Xu, X.; Zhou, S.; Han, J.; Gan, L.; Zhai, T., Strain-sensitive Ferromagnetic Two-dimensional Cr₂Te₃. *Nano Research* **2021**, *15*, 1254-1259.
- (65) Katmis, F.; Lauter, V.; Nogueira, F. S.; Assaf, B. A.; Jamer, M. E.; Wei, P.; Satpati, B.; Freeland, J. W.; Eremin, I.; Heiman, D.; Jarillo-Herrero, P.; Moodera, J. S., A Hightemperature Ferromagnetic Topological Insulating Phase by Proximity Coupling. *Nature* **2016**, *533*, 513-6.
- (66) Zhang, L.; Huang, X.; Dai, H.; Wang, M.; Cheng, H.; Tong, L.; Li, Z.; Han, X.; Wang, X.; Ye, L.; Han, J., Proximity-Coupling-Induced Significant Enhancement of Coercive Field and Curie Temperature in 2D van der Waals Heterostructures. *Adv Mater* **2020**, *32*, e2002032. (67) Tong, Q.; Liu, F.; Xiao, J.; Yao, W., Skyrmions in the Moire of van der Waals 2D Magnets. *Nano Lett* **2018**, *18*, 7194-7199.

For Table of Contents Only:

Quantum Magnetic Image of Thin Co-Fe₅GeTe₂ Flakes



^{*}The numbers indicate the thicknesses of the flakes.